

LSAM: Asynchronous Distributed Training with Landscape-Smoothed Sharpness-Aware Minimization

Yunfei Teng
yfteng@pku.edu.cn

Sixin Zhang
sixin.zhang@irit.fr

Abstract

While Sharpness-Aware Minimization (SAM) improves generalization in deep neural networks by minimizing both loss and sharpness, it suffers from inefficiency in distributed large-batch training. We present *Landscape-Smoothed* SAM (LSAM), a novel optimizer that preserves SAM’s generalization advantages while offering superior efficiency. LSAM integrates SAM’s adversarial steps with an *asynchronous* distributed sampling strategy, generating an asynchronous distributed sampling scheme, producing a smoothed sharpness-aware loss landscape for optimization. This design eliminates synchronization bottlenecks, accelerates large-batch convergence, and delivers higher final accuracy compared to data-parallel SAM.

1 Introduction

Recent advancements in computer vision and natural language processing have been significantly fueled by meticulously designed optimization methods. In this study, we address the optimization challenge expressed as: $f(x) = \min_{x \in \mathbb{R}^d} \mathbb{E}_{\xi \sim \mathcal{D}} [f(x; \xi)] \approx \frac{1}{n} \sum_{i=1}^n f(x; \xi_i)$, where $f(\cdot; \xi): \mathbb{R}^d \rightarrow \mathbb{R}$ is a differentiable (though potentially nonconvex) loss function. Here, ξ is sampled from an unknown distribution \mathcal{D} (typically representing the data distribution), and x denotes the trainable model parameters. In practice, the objective is often approximated by minimizing the empirical risk over a finite dataset instead. This formulation captures a wide range of machine learning tasks, including least-squares regression, neural network training and simulation of molecular dynamics.

It is widely recognized that deep neural networks are highly nonconvex and challenging to optimize. *Sharpness-Aware Minimization* (SAM) (Foret et al., 2020) improves generalization by simultaneously minimizing the empirical loss and the local *sharpness* of the loss landscape. For model parameters x and objective function f , it first finds the adversarial perturbation $\epsilon(x) = \arg \max_{\|\epsilon\| \leq \rho} f(x + \epsilon)$, then applies a conventional optimizer to minimise the worst-case loss $f(x + \epsilon(x))$, guiding the parameters into wider, flatter minima and thus enhancing generalization.

While SAM delivers significant generalization gains, these improvements deteriorate rapidly as the batch size grows (Andriushchenko and Flammarion, 2022; Wen et al., 2023a; Li et al., 2024). In practice, one therefore resorts to a mini-batch surrogate as $\mathbb{E}_{\xi \sim \mathcal{D}} [f(x + \epsilon(x); \xi)]$. Consequently, confining SAM’s effectiveness to moderate batch sizes (e.g., 128) rather than large-batch regimes. This batch sensitivity fundamentally limits SAM’s scalability in conventional data-parallel distributed settings. Under data parallelism, adding workers forces an unfavorable trade-off: either shrink per-worker batches or balloon global batch sizes—both undermining SAM’s training dynamics and restricting its utility for large-scale distributed training.

Thus, beyond the conventional *data-parallel* scheme, is there any other strategy can enable large-scale distributed training of SAM?

This paper answers that question by introducing *sampling parallelism*—a paradigm that overcomes SAM’s batch-size sensitivity and scales gracefully in distributed settings. Sampling parallelism thus establishes a new conceptual framework that complements existing data parallelism strategies. Although earlier methods such as (Zhang et al., 2015; Chaudhari et al., 2016, 2017; Teng et al., 2019; Dimlioglu and Choromanska, 2024) can be retroactively viewed through this lens, they did not explicitly formulate the idea, nor did they provide optimally tuned implementations.

arXiv:2509.03110v1 [cs.LG] 3 Sep 2025

To establish connections between SAM and modern sampling techniques, we first introduce the *Boltzmann distribution* (Gibbs, 1902). This fundamental distribution assigns state probabilities that decay exponentially with energy. In machine learning contexts, where energy corresponds to a loss function f , this yields:

$$\pi_{\text{SAM}}(x) \propto \exp(-\mathbb{E}_{\xi \sim \mathcal{D}}[f(x + \epsilon(x); \xi)]). \quad (1)$$

This formulation suggests that low-loss states occur with higher probabilities. Later in this paper, we will demonstrate that it constitutes a valid distribution under mild constraints.

Prior work (Chen et al., 2022; Lee et al., 2021; Chaudhari et al., 2016; Huang et al., 2024) demonstrates that convolving the loss landscape with a Gaussian kernel, coupled with appropriate regularization, offers an effective optimization solution. Building on this foundation, we introduce *Landscape-Smoothed SAM* (LSAM)—a novel optimizer specifically designed for scalable and robust distributed learning. LSAM simultaneously enhances the smoothness of landscape and strengthens optimization stability through entropy-enhanced regularization. Our theoretical and empirical analyses confirm LSAM’s compatibility with asynchronous operation, enabling a highly efficient training paradigm.

We contribute: (1) A novel *sampling-parallel* framework for distributed SAM that prevents batch inflation; (2) Demonstration that LSAM unifies SAM’s flat minima and Gaussian smoothing’s deep minima; (3) Theoretical proof that LSAM matches SGD convergence rates; (4) Empirical validation showing LSAM’s superiority over data-parallel SAM and similar distributed methods.

2 Related Work

Classical sampling approaches such as Langevin dynamics (Welling and Teh, 2011), MALA (Grenander and Miller, 1994), and HMC (Neal, 2011) couple gradients with injected noise, while proximal and entropy-smoothed variants enhance scalability in high dimensions (Chen et al., 2022; Lee et al., 2021; Chen et al., 2024). Flatness-oriented optimization evolved from the early observation that wide minima improve generalization (Hochreiter and Schmidhuber, 1997; Keskar et al., 2017) to smoothing techniques such as Entropy-SGD (Chaudhari et al., 2016), diffusion-based perturbations (Zhu et al., 2022; Wen et al., 2023b), and augmentation strategies (Zhang et al., 2018), as well as adversarial formulations like SAM (Foret et al., 2020) and its extensions (Kwon et al., 2021; Kim et al., 2023; Qu et al., 2023). Theory has further tied flatness to PAC-Bayes bounds and spectral properties of the loss (Neyshabur et al., 2017; Andriushchenko and Flammarion, 2023). Efforts to scale SAM efficiently include stochastic perturbations, periodic updates, and adaptive learning rates (Du et al., 2022; Liu et al., 2022; Sun et al., 2023a; Behdin et al., 2023), with AsyncSAM (Jo et al., 2025) overlapping perturbation and update steps, and federated variants adapting SAM to heterogeneous data (Qu et al., 2022; Sun et al., 2023b; Fan et al., 2024; Calderola et al., 2025).

Remark 1. Our approach differs by unifying sampling with SAM through communication-level asynchrony, yielding the first sampling-driven framework for distributed sharpness-aware optimization. Nevertheless, our method still requires double the communication cost, same as the original SAM.

3 Theoretical Analysis

3.1 Formulation

In line with the work of (Foret et al., 2020), we formulate the sharpness-aware minimization (SAM) objective as follows:

$$f_{\text{SAM}}^{\max}(x) = \max_{\|\epsilon\| \leq \rho} f(x + \epsilon) \quad (2)$$

This objective seeks to minimize not just the loss at the current parameters x , but the maximum loss within a small ℓ_2 -ball of radius ρ around x , thereby promoting solutions in flatter regions of the loss landscape that are more robust to perturbations and tend to generalize better.

In practical implementations, the maximization over ϵ is often approximated using a first-order Taylor expansion, leading to the perturbation $\epsilon = \rho \cdot \frac{\nabla f(x)}{\|\nabla f(x)\|}$ (for the ℓ_2 -norm case). To enhance numerical stability and avoid issues like division by zero when the gradient norm is small, this is adjusted to f_{SAM}^{\max} is modified to:

$$f_{\text{SAM}}(x) = f\left(x + \frac{\rho \nabla f(x)}{\|\nabla f(x)\| + \gamma}\right), \quad (3)$$

where $\gamma > 0$ is a small regularization constant. This approximation allows efficient computation via a single additional forward-backward pass to evaluate the perturbed loss, which is then used to compute the gradient for the parameter update.

Building on this, the approximation naturally induces a Boltzmann distribution over the parameters x :

$$\pi_{\text{SAM}}(x) \propto \exp(-f_{\text{SAM}}(x)), \quad (4)$$

assigning higher probability to parameter vectors with lower sharpness-aware loss. Under mild assumptions defined and normalizable, linking SAM to sampling-based techniques in optimization and generative modeling.

Theorem 1 (Score Estimation). *Let $f : \mathbb{R}^d \rightarrow \mathbb{R}$ and $k : \mathbb{R}^d \times \mathbb{R}^d \rightarrow [0, \infty)$ satisfy Assumptions 1 and 2 (in Appendix A), and define*

$$I(y) := \int_{\mathbb{R}^d} e^{-f(T_{\rho, \gamma}(x)) - k(x, y)} dx, \quad \pi_{\text{LSAM}}(y) := \frac{I(y)}{Z_{\rho, \gamma} Z}.$$

Assume: (i) $\nabla_y k(x, y)$ exists $\forall (x, y) \in \mathbb{R}^d \times \mathbb{R}^d$; (ii) f is bounded below; (iii) $\|\nabla_y k(x, y)\| \leq g(x)$ for some integrable $g : \mathbb{R}^d \rightarrow \mathbb{R}$. Then differentiation under the integral is valid, and

$$\nabla_y \log \pi_{\text{LSAM}}(y) = -\mathbb{E}_{x \sim q(\cdot | y)} [\nabla_y k(x, y)], \quad q(x | y) = \frac{e^{-f(T_{\rho, \gamma}(x)) - k(x, y)}}{I(y)}. \quad (5)$$

Thus, the log-density gradient equals the negative posterior mean of $\nabla_y k(x, y)$ under q .

Remark 2. Our contribution generalizes prior work (Huang et al., 2024; Chen et al., 2024; Chaudhari et al., 2016) by broadening their findings to encompass general kernels, extending beyond the Gaussian setting. The key observation is that the score at any point y arises from kernel-weighted averages over contributions from its neighbor.

Following prior work (Chaudhari et al., 2016), we adopt a *Gaussian kernel* in our implementation. Under this formulation, π_{LSAM} integrates the adversarial robustness of SAM—which encourages flatter minima by maximizing over worst-case perturbations—with kernel smoothing. The latter alleviates irregularities in the optimization landscape by convolving the loss surface.

Remark 3. Despite its sharpness-aware objective, SAM is often used as merely a first-order optimizer like gradient descent, potentially susceptible to flat yet shallow minima. We demonstrate, however, that SAM fundamentally reshapes the probability landscape. When integrated into our framework as LSAM—which implicitly incorporates zero-order information—SAM can be strategically guided to deeper minima, transcending its traditional role as a standalone optimizer.

3.2 Convergence Rate

In this section, we analyze the convergence behavior of LSAM towards the minima. We first present the algorithmic framework, then derive convergence guarantees for ESGD, and ultimately show that LSAM attains the same convergence rate as classical SGD in approaching stationary points of the objective f .

We cast the optimization procedure an alternating update scheme driven by stochastic gradients. The iterative routines for both ESGD and LSAM are characterized in Algorithm 1. Then, under Assumption 3 and through Algorithm 1, we prove G_t convergence for both: (i) ESGD without perturbation (Theorem 2), and (ii) LSAM with constant and decaying perturbations (Theorem 3 and Theorem 4, respectively). All proofs of this Sections 3.1 and 3.2 are deferred to Appendix B.

Assumption 3 (Stochastic-gradient oracle). Consider the following conditions:

- (C1) **Bounded variance.** There exists $\sigma \geq 0$ such that $\mathbb{E}_{\xi} [\|f(x; \xi) - \nabla f(x)\|^2] \leq \sigma^2$, $\forall x \in \mathbb{R}^d$.
- (C2) **L -smoothness.** There exists $L \geq 0$ such that $\|\nabla f(x_1) - \nabla f(x_2)\| \leq L \|x_1 - x_2\|$, $\forall x_1, x_2$.
- (C3) **Stochastic L -smoothness.** There exists $L \geq 0$ such that for a.e. ξ , $f(\cdot; \xi)$ satisfies L -smoothness in (C2) $\|\nabla f(x_1; \xi) - \nabla f(x_2; \xi)\| \leq L \|x_1 - x_2\|$, $\forall x_1, x_2 \in \mathbb{R}^d$.

Algorithm 1: One-step LSAM / ESGD Update

Select a coupling parameter $\lambda \geq 0$, a mixing coefficient $\alpha \in (0, 1]$, and a sequence of step sizes $\eta_t = \eta_0 / \sqrt{t+1}$ for some $\eta_0 > 0$. The algorithm produces the following updates:

$$x_{t+1} = x_t - \eta_t (g_t + \lambda(x_t - y_t)), \quad (6)$$

$$y_{t+1} = \alpha x_{t+1} + (1 - \alpha) y_t, \quad (7)$$

where g_t is a stochastic gradient which depends on an i.i.d random sample $\xi_t \sim \mathcal{D}$. For convenience, we define:

$$G_t := \nabla f(x_t) + \lambda(x_t - y_t).$$

Comment. Informally, repeatedly applying Equations Equations (6) and (7) in alternation with appropriate injected noise produces updates analogous to a discrete-time Gibbs sampler. In contrast, for optimization we perform each update just once in a sequential recursive schedule.

(C4) **Bounded stochastic gradient norm.** The expected norm of the stochastic gradient is uniformly bounded $\exists C \geq 0$ such that $\mathbb{E}_\xi \|\nabla f(x; \xi)\| \leq C, \forall x \in \mathbb{R}^d$.

Theorem 2 (Convergence of G_t without Perturbation). *Under (C1)-(C2) of Assumption 3, consider the updates with $g_t = \nabla f(x_t; \xi_t)$ with $\eta_0 \leq 1/(L + \lambda)$. Assume f is bounded below. Then the average squared norm of G_t satisfies $\frac{1}{T} \sum_{t=0}^{T-1} \mathbb{E}[\|G_t\|^2] = \mathcal{O}\left(\frac{\log T}{\sqrt{T}}\right)$.*

Theorem 3 (Convergence of G_t with Constant Perturbation). *Under (C1) - (C3) of Assumption 3, consider the updates with $g_t = \nabla f\left(x_t + \rho \frac{\nabla f(x_t; \xi_t)}{\|\nabla f(x_t; \xi_t)\| + \gamma}; \xi_t\right)$ with $\eta_0 \leq \frac{1}{4(L+\lambda)}$. Assume f is bounded below and pick up a constant $\rho > 0$. Then the average squared norm of G_t satisfies: $\frac{1}{T} \sum_{t=0}^{T-1} \mathbb{E}[\|G_t\|^2] \leq 4L^2 \rho^2 + \mathcal{O}\left(\frac{\log T}{\sqrt{T}}\right)$, and thus converges to a neighborhood of size $\mathcal{O}(\rho^2)$.*

Theorem 4 (Convergence with Decaying Perturbation). *Under (C1)-(C3) of Assumption 3, consider the updates with $g_t = \nabla f\left(x_t + \rho_t \frac{\nabla f(x_t; \xi_t)}{\|\nabla f(x_t; \xi_t)\| + \gamma}; \xi_t\right)$ with $\eta_0 \leq \frac{1}{4(L+\lambda)}$. Assume f is bounded below and let $\rho_t = \rho_0/\sqrt{t+1}$ for some $\rho_0 > 0$. Then the average squared norm of G_t satisfies: $\frac{1}{T} \sum_{t=0}^{T-1} \mathbb{E}[\|G_t\|^2] \leq \mathcal{O}\left(\frac{\log T}{\sqrt{T}}\right)$, and thus converges to zero as $T \rightarrow \infty$.*

Theorems 2 to 4 guarantee the convergence of $\|G_t\|$ but not necessarily $\|\nabla f(x_t)\|$. Next, we require (C4) of Assumption 3 and prove the corresponding result in Lemma 5.

Lemma 5 (Decay of the anchor gap). *Let (C1) - (C4) of Assumption 3 hold, and let the iterates $\{(x_t, y_t)\}_{t \geq 0}$ be generated by Algorithm 1 with the g_t in Theorem 2 (resp. Theorem 4). Set $\lambda > 0$ and choose $D \geq C/\lambda$ (resp. $D \geq (C + \rho_0 L)/\lambda$). Assume step sizes $\eta_t = \eta_0/\sqrt{t+1}$ for $\eta_0 > 0$, and initial gap $\|z_0\| \leq D$, where $z_t := x_t - y_t$. Then, for all $t \geq 0$, the norm of z_t remains bounded as $\|z_t\| \leq D$. Moreover, $\mathbb{E}[\|z_t\|^2] = \mathcal{O}(1/\sqrt{t})$ and $\lim_{t \rightarrow \infty} \mathbb{E}[\|z_t\|^2] = 0$.*

Corollary 6 (Gradient norm convergence). *Let (C1) - (C4) of Assumption 3 hold and assume the conditions of Lemma 5 are satisfied. Then for ESGD (resp. LSAM with decaying perturbation) which satisfy the extra assumptions in Theorem 2 (resp. Theorem 4), the expected squared gradient norm satisfies: $\frac{1}{T} \sum_{t=1}^T \mathbb{E}[\|\nabla f(x_t)\|^2] = \mathcal{O}\left(\frac{\log T}{\sqrt{T}}\right)$.*

SAM's convergence analysis shows distinct behaviors: it fails to converge to zero with a fixed ρ stochastically, but converges with a decaying ρ . We prove that LSAM matches SAM's convergence rate for both constant adversarial parameters (Si and Yun, 2023) and a decaying adversarial factor (Andriushchenko and Flammarion, 2022; Li et al., 2024).

4 Algorithm

In this section, we broaden the algorithmic structure presented in Algorithm 1 to encompass a distributed optimization environment, by incorporating sampling and acceleration methodologies to proficiently locate the modes of $\pi_{\text{LSAM}}(y)$ that exhibit strong generalization capabilities. The dual-loop structure comprises two tightly coupled components: (i) An *inner* sampling loop that leverages Langevin Markov chain Monte Carlo (MCMC) methods (Welling and Teh, 2011) to efficiently explore the parameter space and (ii) an *outer* optimization loop that applies a gradient descent mechanism (Bottou, 1998) to push the parameters toward optimal solutions. We elaborate on each component in the subsequent subsections.

Algorithm 2: Asynchronous Distributed LSAM

```

1: Inputs: pulling coefficient  $\lambda$ , perturbation
   radius  $\rho$ , learning rates for sampling and
   optimization  $(\eta, \eta')$ , sync period  $\tau$ , and
   momentum factor  $\beta$ .
2: Initialization: Randomly initialize
   parameters for each worker  $\{x_0^{(i)}\}_{i=1}^n$  and
   the global center  $y_0$ ; set local counters
    $t_x^{(i)} \leftarrow 0$  and global counter  $t_y \leftarrow 0$ .
3: while not converged do
4:   % Asynchronous sampling step
5:   for all  $i = 1, 2, \dots, n$  in parallel do
6:      $s_{t_x^{(i)}}^{(i)} \leftarrow \nabla_x \log q_{x|y}(x_{t_x^{(i)}}^{(i)}; y_{t_y})$ 
7:      $x_{t_x^{(i)}+1}^{(i)} \leftarrow \text{SAMPLER}\left(x_{t_x^{(i)}}^{(i)}, s_{t_x^{(i)}}^{(i)}, \eta\right)$ 
8:      $t_x^{(i)} \leftarrow t_x^{(i)} + 1$ 
9:   end for
10:
11:  % Synchronous optimization step
12:  if  $\sum_{i=1}^n t_x^{(i)} \bmod n\tau = 0$  then
13:     $g'_{t_y} \leftarrow \frac{1}{n\tau} \sum_{i=1}^n \sum_{s=1}^{t_x^{(i)}} x_s^{(i)} - y_{t_y}$ 
14:     $g_{t_y} \leftarrow g'_{t_y} + \beta(g'_{t_y} - g'_{t_y-1})$ 
15:     $y_{t_y+1} \leftarrow \text{OPTIMIZER}(y_{t_y}, g_{t_y}, \eta')$ 
16:     $t_y \leftarrow t_y + 1$ ; reset all  $t_x^{(i)} \leftarrow 0$ 
17:  end if
18: end while

```

4.1 Langevin Dynamics for Sampling

Since the score $\nabla \log \pi_{\text{LSAM}}(y)$ in Theorem 1 does not admit a closed-form computation—owing to the intractable partition function and the convolution integral—we generate samples from the target density via MCMC techniques, chiefly Metropolis–Hastings (Metropolis et al., 1953) or its stochastic-gradient counterpart, Stochastic Gradient Langevin Dynamics (SGLD) (Welling and Teh, 2011). To alleviate the overhead associated with sampling, one could instead directly minimize a proximal approximation of the entropy-regularized objective using standard stochastic optimizers (e.g., SGD or Adam), as suggested in (Chaudhari et al., 2016, 2017), which inherently embeds the smoothing through repeated updates.

4.2 Acceleration Techniques for Optimization

Modern optimization has developed accelerated methods that substantially improve convergence, evolving along a consistent trajectory, illustrated by shifts Momentum SGD to Nesterov’s Accelerated Gradient Descent (AGD) (Nesterov, 1983), Adam (Kingma and Ba, 2015) to Adan (Xie et al., 2024), and ISTA (Daubechies et al., 2004) to FISTA (Beck and Teboulle, 2009). We incorporate their *look-ahead* gradient characteristics via the surrogate direction:

$$g'_t = \nabla_y \log \pi_{\text{LSAM}}(y_t) = -\mathbb{E}_{x \sim q(\cdot|y_t)} [\nabla_y k(x, y_t)] \quad (8)$$

followed by the Adan-AGD-style update (Xie et al., 2024) $g_t \leftarrow g'_t + \beta \cdot (g'_t - g'_{t-1})$, where β is the momentum parameter. The momentum-augmented g_t proactively anticipates future gradients through the change of gradient $(g'_t - g'_{t-1})$.

4.3 Distributed Training

We use Nesterov momentum (Nesterov, 1983) in both the inner sampling loop and the outer optimization step. The gradient $g_{t,y}$ is obtained directly from the aggregation of the asynchronously generated samples from all workers. This setup constitutes a two-time-scale stochastic approximation (Doan, 2023; Chen et al., 2025).

Our algorithm supports fully parallel execution, enabling scalable distributed training. Each worker independently generates samples in parallel, adhering to the conditional distribution in Equation (5). After accumulating $n\tau$ iterations across all workers, synchronization occurs to compute the LSAM score according to Equation (5) and deliver the resulting gradient to the optimizer. This forms the complete workflow of distributed LSAM, detailed in Algorithm 2.

5 Experiments

We compare LSAM with LSGD (Teng et al., 2019), EASGD (Zhang et al., 2015), and the standard data-parallel SGD and SAM method. For empirical experiments, we leverage the SVHN (Netzer et al., 2011), CIFAR-10 and CIFAR-100 datasets (Krizhevsky and Hinton, 2009). On SVHN, we employ CNN-5 (a 5-layer convolutional neural network (LeCun et al., 1998; Krizhevsky et al., 2012)) and ResNet-18 (He et al., 2016). For CIFAR-10, assessments are performed with VGG-16 (Simonyan and Zisserman, 2014), ResNet-20 and WRN-16×10 (Zagoruyko and Komodakis, 2016); and for CIFAR-100, we utilize ResNet-34, WRN-28×10 and WRN-40×10.

5.1 Distributed Architecture

We use a distributed architecture the same as (Teng et al., 2022; Dimlioglu and Choromanska, 2024), featuring a global server and several local servers that synchronize via GLOO for CPU coordination, alongside workers employing NCCL for GPU communication. This architecture only requires naive PyTorch with its build-in distributed training library. This hierarchical configuration facilitates scalable multi-machine, multi-GPU training, with the global server managing aggregations across

Method	CNN-5	ResNet-18
LSAM	4.62	3.04
LSGD	5.47	3.75
EASGD	5.48	3.43
DP-SGD	6.25	3.63
DP-SAM	4.84	3.49

Table 1: Lowest test errors (%) on SVHN.

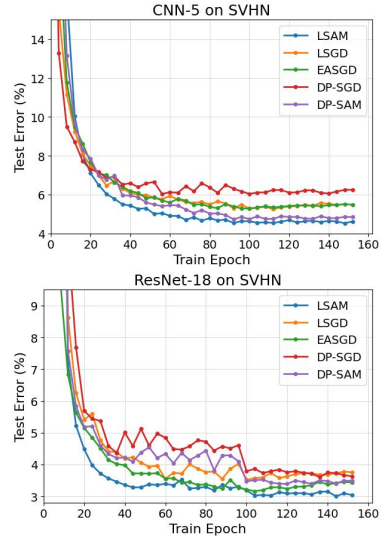


Figure 1: Test error versus training epoch on SVHN. The zoomed plots are in Figure 5, Appendix E.

Method	CIFAR-10			CIFAR-100		
	VGG-16	ResNet-20	WRN-16×10	ResNet-34	WRN-28×10	WRN-40×10
LSAM	6.50	8.15	5.32	31.46	23.75	23.66
LSGD	7.72	9.48	6.12	34.82	24.22	24.03
EASGD	7.76	9.57	6.25	33.24	25.47	25.11
DP-SGD	7.33	9.97	5.87	33.95	24.22	24.94
DP-SAM	7.08	8.89	5.70	32.36	24.41	24.35

Table 2: Lowest test errors (%) on CIFAR-10 and CIFAR-100 datasets.

machines, local servers overseeing intra-node activities, and workers executing parallel GPU operations, accommodating both *asynchronous* and *synchronous* updates. Further details are in Appendix C.

5.2 Experiment Setup

For baselines, we utilize Pytorch’s DataParallel (Paszke et al., 2019) for SGD and SAM, denoted as DP-SGD and DP-SAM, respectively, which synchronously aggregate gradients from all workers for each iteration. We also incorporate asynchronous versions of EASGD and LSGD, which perform local updates for a few steps before synchronization.

More specifically, for DP-SGD and DP-SAM, the communication interval is $\tau = 1$. In contrast, EASGD, LSGD, and our proposed LSAM operate asynchronously with a communication interval of $\tau = 16$. Across all SVHN, CIFAR-10 and CIFAR-100 experiments, we utilize $n = 4$ workers, each with a per-worker batch size of 128. Details of hyperparameter tuning are in Appendix D. All methods are trained for 150 epochs, with the learning rate reduced by a factor of 0.1 at the 100th epoch, aligning with a reduction in test error.

5.3 Results

The lowest test errors across workers and the error–epoch curves for SVHN are shown in Table 1 and Figure 1, where LSAM clearly outperforms all baselines. This trend is reinforced in Table 2 and Figure 2, highlighting LSAM’s markedly faster convergence. Across all dataset–architecture settings, LSAM consistently achieves lower final error and faster convergence than competing methods.

6 Conclusion

We introduce LSAM, a reformulation of SAM that unifies its interpretation as both an optimization and a sampling procedure, specifically tailored for asynchronous distributed training. LSAM achieves faster convergence and improved generalization, while reducing communication overhead and preserving the theoretical guarantees and empirical advantages of SAM.

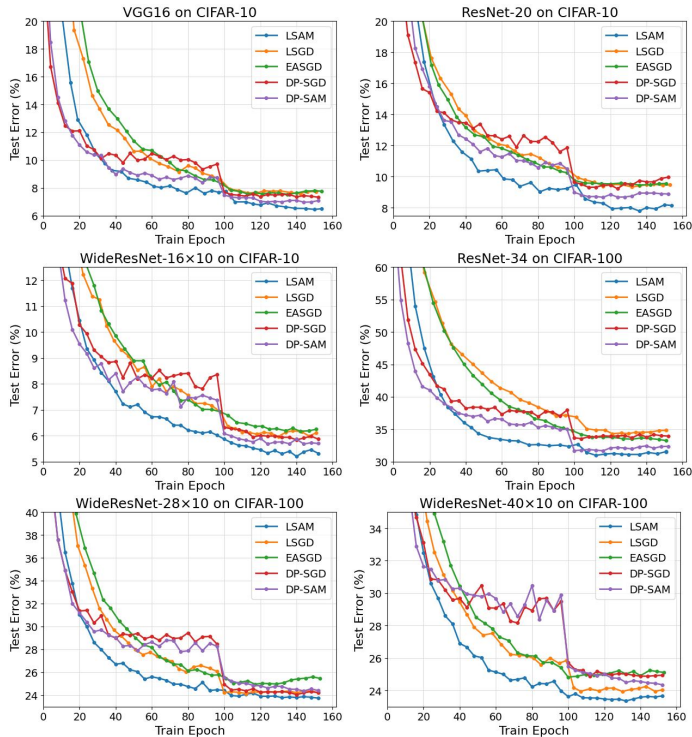


Figure 2: Test error versus training epoch on CIFAR-10 and CIFAR-100 datasets. The zoomed plots are in Figure 6, Appendix E.

References

Maksym Andriushchenko and Nicolas Flammarion. Towards understanding sharpness-aware minimization. In Kamalika Chaudhuri, Stefanie Jegelka, Le Song, Csaba Szepesvari, Gang Niu, and Sivan Sabato, editors, *Proceedings of the 39th International Conference on Machine Learning*, volume 162 of *Proceedings of Machine Learning Research*, pages 639–668. PMLR, 17–23 Jul 2022.

Maksym Andriushchenko and Nicolas Flammarion. Tensor programs v: Tuning large neural networks via zero-shot hyperparameter transfer. *JMLR*, 2023.

Amir Beck and Marc Teboulle. A fast iterative shrinkage-thresholding algorithm for linear inverse problems. *SIAM Journal on Imaging Sciences*, 2(1):183–202, 2009.

Kayhan Behdin, Qingquan Song, Aman Gupta, Sathiya Keerthi, Ayan Acharya, Borja Ocejo, Gregory Dexter, Rajiv Khanna, David Durfee, and Rahul Mazumder. msam: Micro-batch-averaged sharpness-aware minimization, 2023. URL <https://arxiv.org/abs/2302.09693>.

L. Bottou. Online algorithms and stochastic approximations. In *Online Learning and Neural Networks*. Cambridge University Press, 1998.

Debora Caldarola, Pietro Cagnasso, Barbara Caputo, and Marco Ciccone. Beyond local sharpness: Communication-efficient global sharpness-aware minimization for federated learning. In *Proceedings of the IEEE/CVF Conference on Computer Vision and Pattern Recognition (CVPR)*, pages 25187–25197, June 2025.

Pratik Chaudhari, Anna Choromanska, Stefano Soatto, Yann LeCun, Carlo Baldassi, Christian Borgs, Jennifer Chayes, Levent Sagun, and Riccardo Zecchina. Entropy-SGD: Biasing gradient descent into wide valleys. *arXiv preprint arXiv:1611.01838*, 2016.

Pratik Chaudhari, Carlo Baldassi, Riccardo Zecchina, Stefano Soatto, Ameet Talwalkar, and Adam Oberman. Parle: parallelizing stochastic gradient descent. *arXiv preprint arXiv:1707.00424*, 2017.

Wenlin Chen, Mingtian Zhang, Brooks Paige, José Miguel Hernández-Lobato, and David Barber. Diffusive Gibbs sampling. In Ruslan Salakhutdinov, Zico Kolter, Katherine Heller, Adrian Weller, Nuria Oliver, Jonathan Scarlett, and Felix Berkenkamp, editors, *Proceedings of the 41st International Conference on Machine Learning*, volume 235 of *Proceedings of Machine Learning Research*, pages 7731–7747. PMLR, 21–27 Jul 2024. URL <https://proceedings.mlr.press/v235/chen24be.html>.

Yongxin Chen, Sinho Chewi, Adil Salim, and Andre Wibisono. Improved analysis for a proximal algorithm for sampling. In Po-Ling Loh and Maxim Raginsky, editors, *Proceedings of Thirty Fifth Conference on Learning Theory*, volume 178 of *Proceedings of Machine Learning Research*, pages 2984–3014. PMLR, 02–05 Jul 2022. URL <https://proceedings.mlr.press/v178/chen22c.html>.

Zixi Chen, Yumin Xu, and Ruixun Zhang. Convergence rate in a nonlinear two-time-scale stochastic approximation with state (time)-dependence. *Proceedings of the AAAI Conference on Artificial Intelligence*, 39(15):15993–16000, Apr. 2025. doi: 10.1609/aaai.v39i15.33756. URL <https://ojs.aaai.org/index.php/AAAI/article/view/33756>.

Ingrid Daubechies, Michel Defrise, and Christine De Mol. An iterative thresholding algorithm for linear inverse problems with a sparsity constraint. *Communications on Pure and Applied Mathematics*, 57(11):1413–1457, 2004.

Tolga Dimlioglu and Anna Choromanska. Grawa: Gradient-based weighted averaging for distributed training of deep learning models. In Sanjoy Dasgupta, Stephan Mandt, and Yingzhen Li, editors, *Proceedings of The 27th International Conference on Artificial Intelligence and Statistics*, volume 238 of *Proceedings of Machine Learning Research*, pages 2251–2259. PMLR, 02–04 May 2024. URL <https://proceedings.mlr.press/v238/dimlioglu24a.html>.

Thinh T. Doan. Nonlinear two-time-scale stochastic approximation: Convergence and finite-time performance. *IEEE Transactions on Automatic Control*, 68(8):4695–4705, 2023. doi: 10.1109/TAC.2022.3210147.

Jiawei Du, Hanshu Yan, Jiashi Feng, Joey Tianyi Zhou, Liangli Zhen, Rick Siow Mong Goh, and Vincent Tan. Efficient sharpness-aware minimization for improved training of neural networks. In *International Conference on Learning Representations*, 2022. URL <https://openreview.net/forum?id=n00eTdNRG0Q>.

Ziqing Fan, Shengchao Hu, Jiangchao Yao, Gang Niu, Ya Zhang, Masashi Sugiyama, and Yanfeng Wang. Locally estimated global perturbations are better than local perturbations for federated sharpness-aware minimization. In *Proceedings of the 41st International Conference on Machine Learning*, ICML’24. JMLR.org, 2024.

Gerald B. Folland. *Real Analysis: Modern Techniques and Their Applications*. John Wiley & Sons, New York, NY, 2 edition, 1999. ISBN 978-0-471-25032-7.

Pierre Foret, Ariel Kleiner, Hossein Mobahi, and Behnam Neyshabur. Sharpness-aware minimization for efficiently improving generalization, 2020. URL <http://arxiv.org/abs/2010.01412>. cite arxiv:2010.01412.

J. Willard Gibbs. *Elementary Principles in Statistical Mechanics*. Charles Scribner’s Sons, 1902.

Ulf Grenander and Michael I. Miller. Representations of Knowledge in Complex Systems. *Journal of the Royal Statistical Society. Series B (Methodological)*, 56(4):549–603, 1994. ISSN 00359246.

Kaiming He, Xiangyu Zhang, Shaoqing Ren, and Jian Sun. Deep residual learning for image recognition. In *Proceedings of the IEEE conference on computer vision and pattern recognition*, pages 770–778, 2016.

Sepp Hochreiter and Jürgen Schmidhuber. Flat minima. *Neural Computation*, 9(1):173–186, 1997.

Xunpeng Huang, Hanze Dong, Yifan HAO, Yian Ma, and Tong Zhang. Reverse diffusion monte carlo. In *The Twelfth International Conference on Learning Representations*, 2024. URL <https://openreview.net/forum?id=kIPEyMSdFV>.

Junhyuk Jo, Jihyun Lim, and Sunwoo Lee. Asynchronous sharpness-aware minimization for fast and accurate deep learning, 2025. URL <https://arxiv.org/abs/2503.11147>.

Nitish Shirish Keskar, Dheevatsa Mudigere, Jorge Nocedal, Mikhail Smelyanskiy, and Ping Tak Peter Tang. On large-batch training for deep learning: Generalization gap and sharp minima. In *ICLR*, 2017.

Dongjun Kim, Jaeho Park, and Jinwoo Shin. Smooth minima: A convex relaxation framework for optimizing flatness. *AISTATS*, 2023.

Diederik Kingma and Jimmy Ba. Adam: A method for stochastic optimization. In *International Conference on Learning Representations (ICLR)*, San Diego, CA, USA, 2015.

Alex Krizhevsky and Geoffrey Hinton. Learning multiple layers of features from tiny images. Technical report, University of Toronto, 2009. URL <https://www.cs.toronto.edu/~kriz/>.

Alex Krizhevsky, Ilya Sutskever, and Geoffrey E. Hinton. Imagenet classification with deep convolutional neural networks. In *Advances in Neural Information Processing Systems*, volume 25, pages 1097–1105, 2012.

Jungmin Kwon, Jeongseop Kim, Hyunseo Park, and In Kwon Choi. Asam: Adaptive sharpness-aware minimization for scale-invariant learning of deep neural networks. In *ICML*, pages 5905–5914, 2021.

Yann LeCun, Léon Bottou, Yoshua Bengio, and Patrick Haffner. Gradient-based learning applied to document recognition. *Proceedings of the IEEE*, 86(11):2278–2324, 1998. doi: 10.1109/5.726791.

Yin Tat Lee, Ruoqi Shen, and Kevin Tian. Structured logconcave sampling with a restricted gaussian oracle. In Mikhail Belkin and Samory Kpotufe, editors, *Proceedings of Thirty Fourth Conference on Learning Theory*, volume 134 of *Proceedings of Machine Learning Research*, pages 2993–3050. PMLR, 15–19 Aug 2021. URL <https://proceedings.mlr.press/v134/lee21a.html>.

Bolian Li and Ruqi Zhang. Entropy-MCMC: Sampling from flat basins with ease. In *The Twelfth International Conference on Learning Representations*, 2024. URL <https://openreview.net/forum?id=oGNdBvymod>.

Tao Li, Pan Zhou, Zhengbao He, Xinwen Cheng, and Xiaolin Huang. Friendly sharpness-aware minimization. In *Proceedings of the IEEE/CVF Conference on Computer Vision and Pattern Recognition (CVPR)*, pages 5631–5640, June 2024.

Yong Liu, Siqi Mai, Xiangning Chen, Cho-Jui Hsieh, and Yang You. Towards efficient and scalable sharpness-aware minimization, 2022. URL <https://arxiv.org/abs/2203.02714>.

Nicholas Metropolis, Arianna W. Rosenbluth, Marshall N. Rosenbluth, Augusta H. Teller, and Edward Teller. Equation of state calculations by fast computing machines. *The Journal of Chemical Physics*, 21(6):1087–1092, 1953.

Radford M. Neal. *MCMC Using Hamiltonian Dynamics*. May 2011. doi: 10.1201/b10905.

Yurii Nesterov. A method for solving a convex programming problem with convergence rate $\mathcal{O}(1/k^2)$. *Soviet Mathematics Doklady*, 27:372–376, 1983.

Yuval Netzer, Tao Wang, Adam Coates, A. Bissacco, Bo Wu, and A. Ng. Reading digits in natural images with unsupervised feature learning. 2011. URL <https://api.semanticscholar.org/CorpusID:16852518>.

Behnam Neyshabur, Srinadh Bhojanapalli, David McAllester, and Nati Srebro. Exploring generalization in deep learning. *NeurIPS*, 30, 2017.

Adam Paszke, Sam Gross, Francisco Massa, Adam Lerer, James Bradbury, Gregory Chanan, Trevor Killeen, Zeming Lin, Natalia Gimelshein, Luca Antiga, et al. Pytorch: An imperative style, high-performance deep learning library. In *Advances in Neural Information Processing Systems 32*, pages 8024–8035, 2019. URL <https://pytorch.org/>.

Zhe Qu, Xingyu Li, Rui Duan, Yao Liu, Bo Tang, and Zhuo Lu. Generalized federated learning via sharpness aware minimization. In Kamalika Chaudhuri, Stefanie Jegelka, Le Song, Csaba Szepesvari, Gang Niu, and Sivan Sabato, editors, *Proceedings of the 39th International Conference on Machine Learning*, volume 162 of *Proceedings of Machine Learning Research*, pages 18250–18280. PMLR, 17–23 Jul 2022. URL <https://proceedings.mlr.press/v162/qu22a.html>.

Zhe Qu, Xiang Li, and Peter Richtárik. Flatsam: Federated learning with sharpness-aware minimization. In *ICLR*, 2023.

Dongkuk Si and Chulhee Yun. Practical sharpness-aware minimization cannot converge all the way to optima. In *Proceedings of the 37th International Conference on Neural Information Processing Systems*, NIPS ’23, Red Hook, NY, USA, 2023. Curran Associates Inc.

Karen Simonyan and Andrew Zisserman. Very deep convolutional networks for large-scale image recognition. *arXiv preprint arXiv:1409.1556*, 2014.

Hao Sun, Li Shen, Qihuang Zhong, Liang Ding, Shixiang Chen, Jingwei Sun, Jing Li, Guangzhong Sun, and Dacheng Tao. Adasam: Boosting sharpness-aware minimization with adaptive learning rate and momentum for training deep neural networks, 2023a. URL <https://arxiv.org/abs/2303.00565>.

Yan Sun, Li Shen, Shixiang Chen, Liang Ding, and Dacheng Tao. Dynamic regularized sharpness aware minimization in federated learning: approaching global consistency and smooth landscape. In *Proceedings of the 40th International Conference on Machine Learning*, ICML’23. JMLR.org, 2023b.

Y. Teng, W. Gao, F. Chalus, A. Choromanska, D. Goldfarb, and A. Weller. Leader stochastic gradient descent for distributed training of deep learning models. In *NeurIPS*, 2019.

Yunfei Teng, Wenbo Gao, Francois Chalus, Anna Choromanska, Donald Goldfarb, and Adrian Weller. Leader stochastic gradient descent for distributed training of deep learning models: Extension, 2022. URL <https://arxiv.org/abs/1905.10395>.

Max Welling and Yee Whye Teh. Bayesian learning via stochastic gradient langevin dynamics. In *Proceedings of the 28th International Conference on International Conference on Machine Learning*, ICML'11, page 681–688, Madison, WI, USA, 2011. Omnipress. ISBN 9781450306195.

Kaiyue Wen, Tengyu Ma, and Zhiyuan Li. How sharpness-aware minimization minimizes sharpness? In *The Eleventh International Conference on Learning Representations*, 2023a. URL <https://openreview.net/forum?id=5spDgWmpY6x>.

Yeming Wen, Kevin Luk, Max Gazeau, Guodong Zhang, Harris Chan, and Jimmy Ba. Sharpness-aware minimization revisited: Weighted sharpness as a regularization term. *NeurIPS*, 36, 2023b.

Xingyu Xie, Pan Zhou, Huan Li, Zhouchen Lin, and Shuicheng Yan. Adan: Adaptive nesterov momentum algorithm for faster optimizing deep models. *IEEE Transactions on Pattern Analysis and Machine Intelligence*, 2024.

Sergey Zagoruyko and Nikos Komodakis. Wide residual networks. *arXiv preprint arXiv:1605.07146*, 2016.

Hongyi Zhang, Moustapha Cisse, Yann N Dauphin, and David Lopez-Paz. mixup: Beyond empirical risk minimization. In *ICLR*, 2018.

S. Zhang, A. Choromanska, and Y. LeCun. Deep learning with elastic averaging SGD. In *NIPS*, 2015.

Chen Zhu, Yu Cheng, Zhe Gan, Siqi Sun, Tom Goldstein, and Jingjing Liu. Diffusion-based adversarial training produces robust models. *ICML*, 2022.

LSAM: Asynchronous Distributed Training with Landscape-Smoothed Sharpness-Aware Minimization for Improved Generalization (Appendix)

A Additional Theorems

Assumption 1. Let $f : \mathbb{R}^d \rightarrow \mathbb{R}$ be a continuously differentiable potential satisfying¹

$$Z_0 := \int_{\mathbb{R}^d} e^{-f(x)} dx < \infty. \quad (9)$$

Fix parameters $\rho > 0$ and $\gamma > 0$ and define the (bounded) *look-back map* as

$$T_{\rho,\gamma}(x) = x + \frac{\rho \nabla f(x)}{\|\nabla f(x)\| + \gamma}, \quad x \in \mathbb{R}^d, \quad (10)$$

together with its *unnormalised density*

$$\tilde{\pi}_{\rho,\gamma}(x) := \exp[-f(T_{\rho,\gamma}(x))], \quad Z_{\rho,\gamma} := \int_{\mathbb{R}^d} \tilde{\pi}_{\rho,\gamma}(x) dx.$$

Additionally, either of the following conditions holds:

- (A1) f is convex, or
- (A2) f is *globally L -Lipschitz* for some $L > 0$, i.e., $|f(y) - f(x)| \leq L\|y - x\|$ for all $x, y \in \mathbb{R}^d$,

Proposition 7 (Existence of normalized density). *Under Assumption 1, one has $0 < Z_{\rho,\gamma} < \infty$. Consequently*

$$\pi_{\text{SAM}}(x) = \pi_{\rho,\gamma}(x) := Z_{\rho,\gamma}^{-1} \tilde{\pi}_{\rho,\gamma}(x) \quad (11)$$

is a well-defined probability density on \mathbb{R}^d .

Remark 4 (Sharper concentration under convexity). Inequality (15) implies $Z_{\rho,\gamma} \leq Z_0$ when f is convex. Thus, the tails of $\pi_{\rho,\gamma}$ never decays *slower* than that of the baseline Gibbs density e^{-f}/Z_0 , meaning $\pi_{\rho,\gamma}$ is more concentrated. The parameter γ prevents division by zero at critical points of f (where the gradient has norm zero).

To construct LSAM objective function, we define the target distribution as the convolution between the sharpness-aware distribution and a kernel-based Gibbs distribution:

$$\pi_{\text{LSAM}}(y) \propto \int \pi_{\text{SAM}}(x) \pi_{\text{kernel}}(x, y) dx. \quad (12)$$

Here, $\pi_{\text{kernel}}(x, y) = \exp(-k(x, y))$ denotes a kernel that encodes similarity between parameters x and y , with $k(x, y)$ typically a positive semi-definite function (e.g., Gaussian) that decays with distance, thereby facilitating local smoothing by emphasizing nearby points in the parameter space.

Assumption 2 (Kernel slice properties). Let $(\mathcal{X}, \mathcal{B}, dx)$ be a σ -finite measure space and let $k : \mathcal{X} \times \mathcal{X} \rightarrow [0, \infty)$ be a measurable function such that

- (B1) **Non-negativity:** $k(x, y) \geq 0$ for all $x, y \in \mathcal{X}$.

- (B2) **Finite, x -independent normalizer:**

$$Z := \int_{\mathcal{X}} \exp(-k(x, y)) dy \in (0, \infty)$$

for every $x \in \mathcal{X}$ with the value Z *independent* of x .

The following proposition demonstrates that a family of stationary kernels, including gaussian kernels and α -stable noise kernels, satisfies Assumption 2.

¹Typical sufficient conditions are $f(x) \rightarrow \infty$ as $\|x\| \rightarrow \infty$ or $f(x) \geq c\|x\|^q$ for some $q > 1$.

Corollary 8 (Tail condition ensuring a finite normalizer; refer to (Folland, 1999, Section 2.7)). *Let $\phi : \mathbb{R}^d \rightarrow [0, \infty)$ be measurable and define the stationary kernel*

$$k(x, y) = \phi(x - y), \quad x, y \in \mathbb{R}^d.$$

If $z := x - y$ and

$$0 < \int_{\mathbb{R}^d} e^{-\phi(z)} dz < \infty, \quad (13)$$

then the normalizing factor $Z(x) = \int_{\mathbb{R}^d} e^{-k(x, y)} dy$ is finite, strictly positive, and independent of x . A simple pair of sufficient tail-growth assumptions guaranteeing (13) are

- (i) (**Polynomial/exponential growth**) there exist constants $c > 0$, $\alpha > 0$ such that $\phi(z) \geq c \|z\|^\alpha$ for all sufficiently large z ;
- (ii) (**Super-logarithmic growth**) there exist $\varepsilon > 0$ and $R > 0$ with $\phi(z) \geq (d + \varepsilon) \log(1 + \|z\|)$ for $\|z\| \geq R$.

Either condition implies $e^{-\phi} \in L^1(\mathbb{R}^d)$.

Remark 5. Classical examples satisfying the proposition include the exponential-power family $\phi(z) = \lambda \|z\|^\alpha$ (Gaussian when $\alpha = 2$), the Matérn class, the Cauchy kernel, and any integrable compact-support radial kernel. Non-stationary kernels, including linear, polynomial, or sigmoid kernels typically *do not* yield a x -independent normalizer and thus require an alternative normalization approach.

We proceed to demonstrate that π_{SAM} is a valid probability distribution and derive the gradient of $\log \pi_{\text{LSAM}}$, referred to as the *score*, as presented in Proposition 9 and Theorem 1.

Proposition 9 (Kernel-modulated density). *Assume $\mathcal{X} = \mathbb{R}^d$ and Assumptions 1 and 2 hold. Define, for $y \in \mathcal{X}$,*

$$\pi_{\text{LSAM}}(y) := \frac{\int_{\mathcal{X}} e^{-f(T_{\rho, \gamma}(x))} e^{-k(x, y)} dx}{Z_{\rho, \gamma} Z}.$$

Then π_{LSAM} is a probability density on $(\mathcal{X}, \mathcal{B}, dy)$; that is, $\pi_{\text{LSAM}}(y) \geq 0$ for every y and $\int_{\mathcal{X}} \pi_{\text{LSAM}}(y) dy = 1$.

We would like understand the benefits of the π_{LSAM} formulation. For comparison, we group PARLE (Chaudhari et al., 2017), EASGD (Zhang et al., 2015) and Entropy-SGD (Chaudhari et al., 2016) under the label *ESGD*, due to their shared mathematical foundation for solving optimization problems. The distributions of SAM and ESGD are denoted as π_{SAM} and π_{ESGD} , respectively.

Motivation As shown in Figure 3, π_{SAM} suppresses probability mass at sharp minima regardless of depth, π_{ESGD} spreads mass outward to concentrate at deep minima regardless of width, while π_{LSAM} achieves a balanced, smoother, and more selective landscape that empirically yields superior generalization. Consequently, both π_{SAM} and π_{LSAM} can circumvent sharp minima, whereas π_{ESGD} , although intended to seek flat minima, could still converge to deep yet sharp regions.

These distributional differences drive parameters toward distinct basins, motivating optimization under π_{LSAM} to target minima that are both wide and deep. Sampling from the proposed distribution is typically attainable using methods like those described in (Welling and Teh, 2011; Li and Zhang, 2024). These method assembles first-order gradient descent techniques. From an optimization standpoint, π_{LSAM} creates a smoother landscape that is less likely to stall at shallow minima, while π_{SAM} remains at risk of getting trapped in such sub-optimal basins.

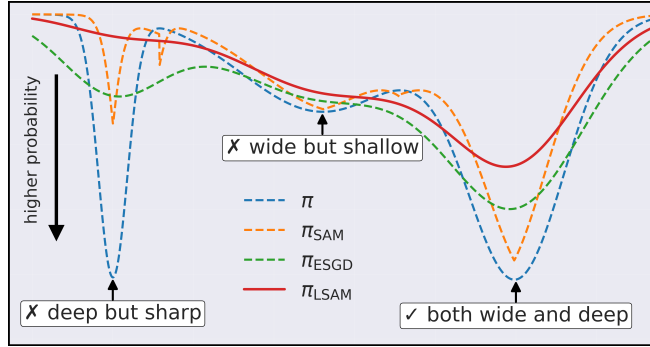


Figure 3: Probability landscapes associated with π , π_{SAM} , π_{ESGD} , and π_{LSAM} . Among the three convergence modes—deep but sharp, wide but shallow, and both wide and deep—ESGD may converge to the first, SAM to the second, whereas LSAM distinctively achieves the third.

B Proofs

B.1 Proofs for Appendix A

Proof of Proposition 7. We take the following steps to show that $0 < Z_{\rho,\gamma} < \infty$ where $Z_{\rho,\gamma} = \int_{\mathbb{R}^d} \tilde{\pi}_{\rho,\gamma}(x) dx$.

Step 1: Positivity and measurability. Since $\varepsilon > 0$, the denominator $\|\nabla f(x)\| + \varepsilon$ is nonvanishing. As f is C^1 , ∇f is continuous, making $T_{\rho,\varepsilon}$ a composition of continuous maps and thus continuous (hence Borel-measurable). The exponential $\exp(\cdot)$ is continuous and positive, so $\tilde{\pi}_{\rho,\varepsilon}(x) > 0$ and Borel-measurable for all x .

Step 2: Uniform bound on the shift. Define $\delta(x) := T_{\rho,\varepsilon}(x) - x$. Then

$$\|\delta(x)\| = \rho \frac{\|\nabla f(x)\|}{\|\nabla f(x)\| + \gamma} \leq \rho \quad \forall x \in \mathbb{R}^d. \quad (14)$$

Step 3: Integrability. We consider the two cases separately.

Case (A1): f convex. By convexity, for all $x \in \mathbb{R}^d$,

$$f(x + \delta(x)) \geq f(x) + \nabla f(x)^\top \delta(x).$$

Substituting $\delta(x)$ and simplifying,

$$\nabla f(x)^\top \delta(x) = \frac{\rho \|\nabla f(x)\|^2}{\|\nabla f(x)\| + \gamma} \geq 0,$$

so $f(x + \delta(x)) \geq f(x)$. Thus,

$$0 < \tilde{\pi}_{\rho,\gamma}(x) = \exp(-f(x + \delta(x))) \leq e^{-f(x)}. \quad (15)$$

Integrating (15) and using finiteness of Z_0 ,

$$0 < Z_{\rho,\gamma} \leq \int_{\mathbb{R}^d} e^{-f(x)} dx = Z_0 < \infty.$$

Case (A2): f globally L -Lipschitz. By the Lipschitz condition and (14),

$$|f(x + \delta(x)) - f(x)| \leq L\|\delta(x)\| \leq L\rho.$$

This implies $f(x + \delta(x)) \geq f(x) - L\rho$, so

$$\tilde{\pi}_{\rho,\gamma}(x) \leq \exp(-f(x) + L\rho) = e^{L\rho} e^{-f(x)}. \quad (16)$$

Integrating (16) and using finiteness of Z_0 ,

$$0 < Z_{\rho,\gamma} \leq e^{L\rho} Z_0 < \infty.$$

Step 4: Normalization. In both cases, $0 < Z_{\rho,\gamma} < \infty$. Thus, $\pi_{\rho,\gamma}(x)$ is non-negative, measurable, and integrates to 1. \square

Proof of Corollary 8. We prove that each condition implies $\int_{\mathbb{R}^d} e^{-\phi(z)} dz < \infty$. For both cases, we split the integral:

$$\int_{\mathbb{R}^d} e^{-\phi(z)} dz = \int_{\|z\| < R} e^{-\phi(z)} dz + \int_{\|z\| \geq R} e^{-\phi(z)} dz,$$

where $R > 0$ is chosen based on the condition. The first integral is always finite since $\|z\| < R$ is compact and $e^{-\phi(z)} \leq 1$:

$$\int_{\|z\| < R} e^{-\phi(z)} dz \leq \text{Vol}(B(0, R)) < \infty.$$

We now prove finiteness of the second integral for each condition.

Condition (i): Assume $\exists c > 0, \alpha > 0, R_0 > 0$ such that $\phi(z) \geq c\|z\|^\alpha$ for $\|z\| \geq R_0$. Take $R = R_0$. Then:

$$\int_{\|z\| \geq R} e^{-\phi(z)} dz \leq \int_{\|z\| \geq R} e^{-c\|z\|^\alpha} dz = S_{d-1} \int_R^\infty r^{d-1} e^{-cr^\alpha} dr.$$

Substitute $t = cr^\alpha$, so $r = (t/c)^{1/\alpha}$, $dr = \frac{1}{\alpha}c^{-1/\alpha}t^{1/\alpha-1}dt$:

$$\int_R^\infty r^{d-1} e^{-cr^\alpha} dr = \frac{1}{\alpha}c^{-d/\alpha} \int_{cR^\alpha}^\infty t^{d/\alpha-1} e^{-t} dt.$$

The integral converges as $t^{d/\alpha-1}e^{-t}$ is integrable at ∞ (upper incomplete gamma function).

Condition (ii): Assume $\exists \varepsilon > 0, R > 0$ such that $\phi(z) \geq (d + \varepsilon) \log(1 + \|z\|)$ for $\|z\| \geq R$. Then:

$$e^{-\phi(z)} \leq (1 + \|z\|)^{-(d+\varepsilon)} \quad \text{for } \|z\| \geq R,$$

so

$$\int_{\|z\| \geq R} e^{-\phi(z)} dz \leq S_{d-1} \int_R^\infty r^{d-1} (1 + r)^{-(d+\varepsilon)} dr.$$

For $r \geq R \geq 1$, $1 + r \leq 2r$, so:

$$r^{d-1} (1 + r)^{-(d+\varepsilon)} \leq r^{d-1} (2r)^{-(d+\varepsilon)} = 2^{-(d+\varepsilon)} r^{-1-\varepsilon}.$$

Thus:

$$S_{d-1} \int_R^\infty r^{d-1} (1 + r)^{-(d+\varepsilon)} dr \leq S_{d-1} 2^{-(d+\varepsilon)} \int_R^\infty r^{-1-\varepsilon} dr = \frac{S_{d-1} 2^{-(d+\varepsilon)}}{\varepsilon R^\varepsilon} < \infty.$$

For both cases, the tail integral converges. Combined with the compact part, $\int_{\mathbb{R}^d} e^{-\phi(z)} dz < \infty$. Strict positivity holds if $\phi \not\equiv \infty$ on a set of positive measure. \square

Proof of Proposition 9. To show that $\pi_{\text{LSAM}}(y)$ is a valid density, we first check that it is non-negative at each $y \in \mathbb{R}^d$ (by the non-negativity of the integrated). Then for normalization, Tonelli's theorem (applied by non-negativity) and Fubini yield:

$$\begin{aligned} \int_{\mathcal{X}} \pi_{\text{LSAM}}(y) dy &= \frac{1}{Z_{\rho,\gamma} Z} \int_{\mathcal{X}} e^{-f(T_{\rho,\gamma}(x))} \underbrace{\left(\int_{\mathcal{X}} e^{-k(x,y)} dy \right)}_Z dx \\ &= \frac{1}{Z_{\rho,\gamma}} \int_{\mathcal{X}} e^{-f(T_{\rho,\gamma}(x))} dx = 1, \end{aligned}$$

where we use $\int_{\mathcal{X}} e^{-k(x,y)} dy = Z$ and $\int_{\mathcal{X}} e^{-f(T_{\rho,\gamma}(x))} dx = Z_{\rho,\gamma}$. Thus $\pi_{\text{LSAM}}(y)$ is a valid density. \square

B.2 Proofs for Section 3.1

Proof of Theorem 1. From the definition $\pi_{\text{LSAM}}(y) = I(y)/(Z_{\rho,\gamma} Z)$, it suffices to obtain the derivative of $I(y)$ to compute the score of π_{LSAM} . We next apply a classical result for differentiation under integral to compute the partial derivative of $I(y)$ with respect to each y_i at $y = (y_i)_{i \leq d} \in \mathbb{R}^d$.

Recall that $I(y) := \int_{\mathbb{R}^d} e^{-f(T_{\rho,\gamma}(x))-k(x,y)} dx$. From the conditions of Theorem 1, we have for any $(x, y) \in \mathbb{R}^d \times \mathbb{R}^d$

$$|\nabla_{y_i} e^{-f(T_{\rho,\gamma}(x))-k(x,y)}| = |e^{-f(T_{\rho,\gamma}(x))-k(x,y)} \nabla_{y_i} k(x, y)| \leq e^{-\min_x f} |\nabla_{y_i} k(x, y)| \leq e^{-\min_x f} g(x),$$

because $f(T_{\rho,\gamma}(x)) \geq \min_x f > -\infty$ and $k(x, y) \geq 0$. It follows from Folland (1999, Theorem 2.27) (extended to unbounded domains for each $y_i \in \mathbb{R}$) that $I(y)$ is differentiable on \mathbb{R}^d , and

$$\begin{aligned} \nabla_y I(y) &= - \int_{\mathbb{R}^d} e^{-f(T_{\rho,\gamma}(x))-k(x,y)} \nabla_y k(x, y) dx \\ &= -I(y) \mathbb{E}_q [\nabla_y k(x, y)]. \end{aligned} \tag{17}$$

From (17) and the definition of q , we obtain

$$\nabla_y \log \pi_{\text{LSAM}}(y) = -\mathbb{E}_{x \sim q(\cdot|y)} [\nabla_y k(x, y)].$$

\square

B.3 Proofs for Section 3.2

Proof of Theorem 2. Define $z_t = x_t - y_t$ and $G_t = \nabla f(x_t) + \lambda z_t$. Consider the Lyapunov function $\Phi_t = f(x_t) + \frac{\lambda}{2} \|z_t\|^2$. Define $F_t(x) = f(x) + \frac{\lambda}{2} \|x - y_t\|^2$. Since f is L -smooth, F_t is L_λ -smooth with $L_\lambda = L + \lambda$, satisfying

$$\|\nabla F_t(x) - \nabla F_t(y)\| \leq L_\lambda \|x - y\|$$

for all $x, y \in \mathbb{R}^d$. Applying this to x_t and x_{t+1} :

$$F_t(x_{t+1}) \leq F_t(x_t) + \langle \nabla F_t(x_t), x_{t+1} - x_t \rangle + \frac{L_\lambda}{2} \|x_{t+1} - x_t\|^2.$$

Substituting the update $x_{t+1} - x_t = -\eta_t(g_t + \lambda z_t)$ and $\nabla F_t(x_t) = G_t$:

$$F_t(x_{t+1}) \leq F_t(x_t) - \eta_t \langle G_t, g_t + \lambda z_t \rangle + \frac{L_\lambda}{2} \eta_t^2 \|g_t + \lambda z_t\|^2.$$

Taking the conditional expectation $\mathbb{E}_t[\cdot] = \mathbb{E}[\cdot | \mathcal{F}_t]$ where \mathcal{F}_t is the σ -field of $(\xi_0, \dots, \xi_{t-1})$:

$$\mathbb{E}_t[F_t(x_{t+1})] \leq F_t(x_t) - \eta_t \|G_t\|^2 + \frac{L_\lambda}{2} \eta_t^2 \mathbb{E}_t[\|g_t + \lambda z_t\|^2],$$

where we used $\mathbb{E}_t[g_t] = \mathbb{E}[\nabla f(x_t; \xi_t) | \mathcal{F}_t] = \nabla f(x_t)$ since x_t depends only on $(\xi_0, \dots, \xi_{t-1})$ (x_t is in the sigma field \mathcal{F}_t) and ξ_t is conditionally independent of x_t given $(\xi_0, \dots, \xi_{t-1})$. Expanding the last term:

$$\begin{aligned} \mathbb{E}_t[\|g_t + \lambda z_t\|^2] &= \mathbb{E}_t[\|(g_t - \nabla f(x_t)) + G_t\|^2] \\ &= \mathbb{E}_t[\|g_t - \nabla f(x_t)\|^2] + \|G_t\|^2 + 2\langle \mathbb{E}_t[g_t - \nabla f(x_t)], G_t \rangle \\ &\leq \sigma^2 + \|G_t\|^2, \end{aligned}$$

by bounded variance assumption. Thus:

$$\mathbb{E}_t[F_t(x_{t+1})] \leq F_t(x_t) - \eta_t \|G_t\|^2 + \frac{L_\lambda}{2} \eta_t^2 (\sigma^2 + \|G_t\|^2).$$

Using the y_{t+1} update and $\Phi_{t+1} = f(x_{t+1}) + \frac{\lambda}{2} \|x_{t+1} - y_{t+1}\|^2$:

$$\begin{aligned} \Phi_{t+1} &= F_t(x_{t+1}) - \frac{\lambda}{2} (1 - (1 - \alpha)^2) \|x_{t+1} - y_t\|^2 \\ &\leq F_t(x_{t+1}) - \frac{\lambda}{2} \alpha \|x_{t+1} - y_t\|^2, \end{aligned}$$

since $1 - (1 - \alpha)^2 \geq \alpha$. Taking conditional expectation:

$$\mathbb{E}_t[\Phi_{t+1}] \leq \mathbb{E}_t[F_t(x_{t+1})] - \frac{\lambda}{2} \alpha \mathbb{E}_t[\|x_{t+1} - y_t\|^2].$$

Combining with previous results:

$$\begin{aligned} \mathbb{E}_t[\Phi_{t+1}] &\leq \Phi_t - \eta_t \|G_t\|^2 + \frac{L_\lambda}{2} \eta_t^2 (\sigma^2 + \|G_t\|^2) - \frac{\lambda}{2} \alpha \mathbb{E}_t[\|x_{t+1} - y_t\|^2] \\ &\leq \Phi_t - \frac{\eta_t}{2} \|G_t\|^2 + \frac{L_\lambda}{2} \eta_t^2 \sigma^2, \end{aligned}$$

using $\eta_t \leq 1/L_\lambda$. Taking total expectation and summing from $t = 0$ to $T - 1$:

$$\sum_{t=0}^{T-1} \frac{\eta_t}{2} \mathbb{E}[\|G_t\|^2] \leq \Phi_0 - \mathbb{E}[\Phi_T] + \frac{L_\lambda \sigma^2}{2} \sum_{t=0}^{T-1} \eta_t^2 \leq \Delta + \frac{L_\lambda \sigma^2}{2} \sum_{t=0}^{T-1} \eta_t^2,$$

where $\Delta = \Phi_0 - \inf_x f(x)$. With $\eta_t = \eta_0 / \sqrt{t+1}$:

$$\forall 0 \leq t \leq T - 1, \eta_t \geq \frac{\eta_0}{\sqrt{T}}, \quad \sum_{t=0}^{T-1} \eta_t^2 \leq \eta_0^2 (1 + \log T).$$

Thus:

$$\frac{1}{T} \sum_{t=0}^{T-1} \mathbb{E}[\|G_t\|^2] \leq \frac{2\Delta + L_\lambda \sigma^2 \eta_0^2 (1 + \log T)}{\eta_0 T} \sqrt{T} = \mathcal{O}\left(\frac{\log T}{\sqrt{T}}\right),$$

and $\lim_{t \rightarrow \infty} \mathbb{E}[\|G_t\|^2] = 0$ follows. \square

Proof of Theorem 3. Define $z_t = x_t - y_t$, $G_t = \nabla f(x_t) + \lambda z_t$, and $\Phi_t = f(x_t) + \frac{\lambda}{2} \|z_t\|^2$. Let $L_\lambda = L + \lambda$. The perturbation is stochastic: $\delta_t = \rho \frac{\nabla f(x_t; \xi_t)}{\|\nabla f(x_t; \xi_t)\| + \gamma}$, so g_t is evaluated at $\tilde{x}_t = x_t + \delta_t$. By L -smoothness and $\|\delta_t\| \leq \rho$:

$$\|\nabla f(\tilde{x}_t) - \nabla f(x_t)\| \leq L\|\delta_t\| \leq L\rho.$$

Start from the smoothness of $F_t(x) = f(x) + \frac{\lambda}{2} \|x - y_t\|^2$:

$$F_t(x_{t+1}) \leq F_t(x_t) + \langle \nabla F_t(x_t), x_{t+1} - x_t \rangle + \frac{L_\lambda}{2} \|x_{t+1} - x_t\|^2.$$

Substitute the update $x_{t+1} - x_t = -\eta_t(g_t + \lambda z_t)$:

$$F_t(x_{t+1}) \leq F_t(x_t) - \eta_t \langle G_t, g_t + \lambda z_t \rangle + \frac{L_\lambda}{2} \eta_t^2 \|g_t + \lambda z_t\|^2.$$

Take conditional expectation:

$$\mathbb{E}_t[F_t(x_{t+1})] \leq F_t(x_t) - \eta_t \langle G_t, \mathbb{E}_t[g_t] + \lambda z_t \rangle + \frac{L_\lambda}{2} \eta_t^2 \mathbb{E}_t[\|g_t + \lambda z_t\|^2]. \quad (18)$$

By (C3), we have $\|\nabla f(x_t + \delta_t; \xi_t) - \nabla f(x_t; \xi_t)\| \leq L\|\delta_t\| \leq L\rho$, therefore

$$\|\mathbb{E}_t[g_t] - \nabla f(x_t)\| \leq L\rho$$

Here, we express the inner product as:

$$\langle G_t, \mathbb{E}_t[g_t] + \lambda z_t \rangle = \|G_t\|^2 + \langle G_t, \mathbb{E}_t[g_t] - \nabla f(x_t) \rangle. \quad (19)$$

Next, we invoke the Cauchy-Schwarz inequality to bound the second term in (19):

$$|\langle G_t, \mathbb{E}_t[g_t] - \nabla f(x_t) \rangle| \leq L\rho \|G_t\|. \quad (20)$$

Expand the variance term:

$$\begin{aligned} \mathbb{E}_t[\|g_t + \lambda z_t\|^2] &= \mathbb{E}_t[\|(g_t - \nabla f(x_t)) + (\nabla f(x_t) + \lambda z_t)\|^2] \\ &= 2\mathbb{E}_t[\|g_t - \nabla f(x_t)\|^2] + 2\|\nabla f(x_t) + \lambda z_t\|^2 \\ &\leq 2\mathbb{E}_t[\|g_t - \nabla f(x_t)\|^2] + 2\|G_t\|_2^2 \end{aligned}$$

To obtain an upper bound of $\mathbb{E}_t[\|g_t - \nabla f(x_t)\|^2]$, we compute from (C3)

$$\begin{aligned} \|g_t - \nabla f(x_t)\|^2 &= \|\nabla f(x_t + \delta_t; \xi_t) - \nabla f(x_t)\|^2 \\ &= \|\nabla f(x_t + \delta_t; \xi_t) - \nabla f(x_t; \xi_t) + \nabla f(x_t; \xi_t) - \nabla f(x_t)\|^2 \\ &\leq 2\|\nabla f(x_t + \delta_t; \xi_t) - \nabla f(x_t; \xi_t)\|^2 + 2\|\nabla f(x_t; \xi_t) - \nabla f(x_t)\|^2 \\ &\leq 2L^2 \rho^2 + 2\|\nabla f(x_t; \xi_t) - \nabla f(x_t)\|^2 \end{aligned}$$

Combine all terms:

$$\begin{aligned} \mathbb{E}_t[\|g_t + \lambda z_t\|^2] &\leq 4L^2 \rho^2 + 4\mathbb{E}_t\|\nabla f(x_t; \xi_t) - \nabla f(x_t)\|^2 + 2\|G_t\|_2^2 \\ &\leq 4L^2 \rho^2 + 4\sigma^2 + 2\|G_t\|_2^2. \end{aligned} \quad (21)$$

Now we bound (18) using (19),(20),(21),

$$\begin{aligned} \mathbb{E}_t[F_t(x_{t+1})] &\leq F_t(x_t) - \eta_t \|G_t\|^2 + \eta_t \langle G_t, \mathbb{E}_t[g_t] - \nabla f(x_t) \rangle + \frac{L_\lambda}{2} \eta_t^2 (4L^2 \rho^2 + 4\sigma^2 + 2\|G_t\|_2^2) \\ &= F_t(x_t) - \eta_t (1 - L_\lambda \eta_t) \|G_t\|^2 + \eta_t L \rho \|G_t\| + 2L_\lambda \eta_t^2 (L^2 \rho^2 + \sigma^2). \end{aligned}$$

Apply Young's inequality to $\eta_t L \rho \|G_t\|$:

$$\eta_t L \rho \|G_t\| \leq \frac{\eta_t}{4} \|G_t\|^2 + \eta_t L^2 \rho^2.$$

With $\eta_t \leq 1/(4L_\lambda)$:

$$\begin{aligned}\mathbb{E}_t[F_t(x_{t+1})] &\leq F_t(x_t) - \eta_t \left(1 - L_\lambda \eta_t - \frac{1}{4}\right) \|G_t\|^2 + \eta_t L^2 \rho^2 + 2L_\lambda \eta_t^2 (L^2 \rho^2 + \sigma^2) \\ &\leq F_t(x_t) - \frac{\eta_t}{2} \|G_t\|^2 + \eta_t L^2 \rho^2 + 2L_\lambda \eta_t^2 (L^2 \rho^2 + \sigma^2).\end{aligned}$$

Relate to Φ_{t+1} :

$$\Phi_{t+1} = F_t(x_{t+1}) - \frac{\lambda}{2} \|x_{t+1} - y_t\|^2 + \frac{\lambda}{2} \|x_{t+1} - y_{t+1}\|^2 \leq F_t(x_{t+1}),$$

Thus:

$$\mathbb{E}_t[\Phi_{t+1}] \leq \mathbb{E}_t[F_t(x_{t+1})] \leq \Phi_t - \frac{\eta_t}{2} \|G_t\|^2 + \eta_t L^2 \rho^2 + 2L_\lambda \eta_t^2 (L^2 \rho^2 + \sigma^2).$$

Take total expectation and sum from $t = 0$ to $T - 1$:

$$\sum_{t=0}^{T-1} \frac{\eta_t}{2} \mathbb{E}[\|G_t\|^2] \leq \Phi_0 - \mathbb{E}[\Phi_T] + L^2 \rho^2 \sum_{t=0}^{T-1} \eta_t + 2L_\lambda \eta_t^2 (L^2 \rho^2 + \sigma^2).$$

Multiply by 2 and set $\Delta = \Phi_0 - \inf_x f(x)$:

$$\sum_{t=0}^{T-1} \eta_t \mathbb{E}[\|G_t\|^2] \leq 2\Delta + 2L^2 \rho^2 \sum_{t=0}^{T-1} \eta_t + 4L_\lambda \eta_t^2 (L^2 \rho^2 + \sigma^2) \sum_{t=0}^{T-1} \eta_t^2.$$

With $\eta_t = \eta_0/\sqrt{t+1}$:

$$\sum_{t=0}^{T-1} \eta_t \leq 2\eta_0 \sqrt{T}, \quad \sum_{t=0}^{T-1} \eta_t^2 \leq \eta_0^2 (1 + \log T).$$

Thus:

$$\sum_{t=0}^{T-1} \eta_t \mathbb{E}[\|G_t\|^2] \leq 2\Delta + 4\eta_0 L^2 \rho^2 \sqrt{T} + 4L_\lambda (L^2 \rho^2 + \sigma^2) \eta_0^2 (1 + \log T).$$

Since $\eta_t \geq \eta_0/\sqrt{T}$ for $0 \leq t \leq T - 1$:

$$\sum_{t=0}^{T-1} \mathbb{E}[\|G_t\|^2] \leq \frac{\sqrt{T}}{\eta_0} \sum_{t=0}^{T-1} \eta_t \mathbb{E}[\|G_t\|^2] \leq \frac{\sqrt{T}}{\eta_0} \left[2\Delta + 4\eta_0 L^2 \rho^2 \sqrt{T} + 4L_\lambda (L^2 \rho^2 + \sigma^2) \eta_0^2 (1 + \log T) \right].$$

Divide by T :

$$\frac{1}{T} \sum_{t=0}^{T-1} \mathbb{E}[\|G_t\|^2] \leq \frac{2\Delta}{\eta_0 \sqrt{T}} + 4L^2 \rho^2 + \frac{4L_\lambda (L^2 \rho^2 + \sigma^2) \eta_0 (1 + \log T)}{\sqrt{T}}.$$

The right-hand side is $4L^2 \rho^2 + \mathcal{O}\left(\frac{\log T}{\sqrt{T}}\right)$, which completes the proof. \square

Proof of Theorem 4. Similar to the constant ρ case, take total expectation and sum from $t = 0$ to $T - 1$:

$$\sum_{t=0}^{T-1} \frac{\eta_t}{2} \mathbb{E}[\|G_t\|^2] \leq \Phi_0 - \mathbb{E}[\Phi_T] + L^2 \sum_{t=0}^{T-1} \eta_t \rho_t^2 + 2L_\lambda \left(L^2 \sum_{t=0}^{T-1} \eta_t^2 \rho_t^2 + \sigma^2 \sum_{t=0}^{T-1} \eta_t^2 \right).$$

Multiply by 2 and set $\Delta = \Phi_0 - \inf_x f(x)$:

$$\begin{aligned}\sum_{t=0}^{T-1} \eta_t \mathbb{E}[\|G_t\|^2] &\leq 2\Delta + 2L^2 \sum_{t=0}^{T-1} \eta_t \rho_t^2 + 4L_\lambda L^2 \sum_{t=0}^{T-1} \eta_t^2 \rho_t^2 + 4L_\lambda \sigma^2 \sum_{t=0}^{T-1} \eta_t^2 \\ &= 2\Delta + 2L^2 \eta_0 \rho_0^2 \sum_{t=0}^{T-1} (t+1)^{-3/2} + 4L_\lambda L^2 \eta_0^2 \rho_0^2 \sum_{t=0}^{T-1} (t+1)^{-2} \\ &\quad + 4L_\lambda \sigma^2 \eta_0^2 \sum_{t=0}^{T-1} (t+1)^{-1} \\ &\leq 2\Delta + 2L^2 \eta_0 \rho_0^2 \zeta(3/2) + 4L_\lambda L^2 \eta_0^2 \rho_0^2 \zeta(2) + 4L_\lambda \sigma^2 \eta_0^2 (1 + \log T)\end{aligned}$$

where $\zeta(\cdot)$ is the Riemann zeta function. Since $\eta_t \geq \eta_0/\sqrt{T}$ for $0 \leq t \leq T-1$:

$$\begin{aligned} \frac{1}{T} \sum_{t=0}^{T-1} \mathbb{E}[\|G_t\|^2] &\leq \frac{1}{\eta_0 \sqrt{T}} \left[2\Delta + 2L^2\eta_0\rho_0^2\zeta(3/2) \right. \\ &\quad \left. + 4L_\lambda L^2\eta_0^2\rho_0^2\zeta(2) + 4L_\lambda\sigma^2\eta_0^2(1+\log T) \right] \\ &= \frac{2\Delta}{\eta_0 \sqrt{T}} + \frac{2L^2\eta_0^2\zeta(3/2)}{\sqrt{T}} + \frac{4L_\lambda L^2\eta_0\rho_0^2\zeta(2)}{\sqrt{T}} + \frac{4L_\lambda\sigma^2\eta_0(1+\log T)}{\sqrt{T}} \end{aligned}$$

The averaged norm $\frac{1}{T} \sum_{t=0}^{T-1} \mathbb{E}[\|G_t\|^2]$ converges to zero as $T \rightarrow \infty$ with rate $\mathcal{O}\left(\frac{\log T}{\sqrt{T}}\right)$. \square

Proof of Lemma 5. Step 1 (uniform bound on $\mathbb{E}\|z_t\|$). The update rule gives

$$z_{t+1} = (1-\alpha)[(1-\lambda\eta_t)z_t - \eta_t g_t].$$

Taking expectations and using the triangle inequality (for LSAM with decaying perturbation in Theorem 4, $G = C + \rho_0 L$ since $\mathbb{E}_t[\|g_t\|] \leq \mathbb{E}_t[\|\nabla f(x_t; \xi_t)\|] + \rho_t L \leq C + \rho_0 L$; for ESGD, $G = C$),

$$\mathbb{E}\|z_{t+1}\| \leq (1-\alpha)[(1-\lambda\eta_t)\mathbb{E}\|z_t\| + \eta_t G].$$

Inductively suppose $\mathbb{E}\|z_t\| < D$. Because $G \leq \lambda D$,

$$(1-\lambda\eta_t)D + \eta_t G \leq (1-\lambda\eta_t)D + \eta_t \lambda D = D,$$

so $\mathbb{E}\|z_{t+1}\| < (1-\alpha)D < D$. The claim follows.

Step 2 (rate for $\mathbb{E}\|z_t\|^2$). Let $d_t = \mathbb{E}\|z_t\|^2$. Squaring the update and expanding,

$$\|z_{t+1}\|^2 = (1-\alpha)^2[(1-\lambda\eta_t)^2\|z_t\|^2 - 2\eta_t(1-\lambda\eta_t)z_t^\top g_t + \eta_t^2\|g_t\|^2].$$

Taking conditional expectations and then full expectations, using $|z_t^\top \mathbb{E}_t[g_t]| \leq \|z_t\| \cdot G$ and $\mathbb{E}\|z_t\| < D$,

$$d_{t+1} \leq (1-\alpha)^2(1-\lambda\eta_t)^2d_t + 2(1-\alpha)^2\eta_t(1-\lambda\eta_t)DG + (1-\alpha)^2\eta_t^2G^2.$$

Set

$$A_t = (1-\alpha)^2(1-\lambda\eta_t)^2, \quad F_t = (1-\alpha)^2[2\eta_t(1-\lambda\eta_t)DG + \eta_t^2G^2].$$

Since $\eta_t^2 \leq \eta_0\eta_t$, there exists a constant $K > 0$ with $F_t \leq K\eta_t$. Iterating the inequality,

$$d_t \leq \left(\prod_{k=0}^{t-1} A_k \right) d_0 + \sum_{k=0}^{t-1} F_k \prod_{j=k+1}^{t-1} A_j.$$

Write $\rho = (1-\alpha)^2 < 1$. Because $A_k \leq \rho$,

$$\prod_{k=0}^{t-1} A_k \leq \rho^t, \quad F_k \leq K\eta_0(k+1)^{-1/2}.$$

Splitting the geometric sum at $k = \lfloor t/2 \rfloor$ shows $\sum_{k=0}^{t-1} F_k \prod_{j=k+1}^{t-1} A_j = \mathcal{O}(t^{-1/2})$, while $\rho^t d_0$ decays exponentially. Hence $d_t = \mathcal{O}(t^{-1/2})$ and $d_t \rightarrow 0$. \square

Proof of Corollary 6. Given the definitions $z_t := x_t - y_t$ and $G_t = \nabla f(x_t) + \lambda z_t$ with asymptotic bounds $\mathbb{E}\|G_t\|^2 = \mathcal{O}\left(\frac{\log T}{\sqrt{T}}\right)$ and $\mathbb{E}\|z_t\|^2 = \mathcal{O}\left(\frac{\log T}{\sqrt{T}}\right)$, we derive the convergence rate for the gradient norm. Starting from the identity $\nabla f(x_t) = G_t - \lambda z_t$, we apply the fundamental inequality $\|a + b\|^2 \leq 2\|a\|^2 + 2\|b\|^2$ to obtain:

$$\|\nabla f(x_t)\|^2 \leq 2\|G_t\|^2 + 2\lambda^2\|z_t\|^2.$$

Taking expectations and substituting the given rates yields:

$$\mathbb{E}\|\nabla f(x_t)\|^2 \leq 2\mathbb{E}\|G_t\|^2 + 2\lambda^2\mathbb{E}\|z_t\|^2.$$

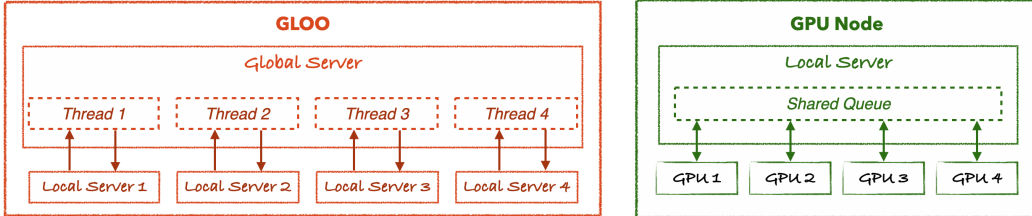


Figure 4: The global server establishes connections with each local server, while local servers communicate with their respective GPUs via thread-safe shared queues to ensure stable operations and reliable communication across the distributed system.

By the asymptotic assumptions, there exist positive constants C_1, C_2 such that for sufficiently large T ,

$$\mathbb{E}\|G_t\|^2 \leq C_1 \frac{\log T}{\sqrt{T}} \quad \text{and} \quad \mathbb{E}\|z_t\|^2 \leq C_2 \frac{\log T}{\sqrt{T}}.$$

Combining these bounds, we conclude:

$$\mathbb{E}\|\nabla f(x_t)\|^2 \leq (2C_1 + 2\lambda^2 C_2) \frac{\log T}{\sqrt{T}} = \mathcal{O}\left(\frac{\log T}{\sqrt{T}}\right).$$

□

C Distributed Training

C.1 Workflow Design

For each local server, the global server spawns a dedicated communication thread. These threads collectively maintain an iteration counter tracking total worker iterations since the last synchronization². At the start of every training iteration, workers send requests to their local servers and await responses. Communication occurs through the following: local servers forward requests to the global server, which evaluates system state and returns responses. The local server then enqueues these responses into worker-accessible queues, enabling workers to dequeue and execute embedded instructions—either local or distributed training—based on the global server’s directives. This entire sequence, depicted in Figure 4, establishes a stable workflow that orchestrates all critical component interactions.

C.2 Batch Normalization

A key difficulty in distributed training is managing the running mean and variance in batch normalization layers. Common strategies either let each worker maintain its own statistics (ignoring synchronization) or introduce extra coordination to sync them. There is no universally optimal approach in asynchronous settings. In our framework—which is built around loosely coupled parameters—we do not synchronize these statistics, and empirical results show no degradation in performance.

C.3 PyTorch Data Loader

In PyTorch, the `dataLoader` by default uses CPU multiprocessing, which can incur overhead from repeatedly spawning and tearing down worker processes. To alleviate this, we enable the `persistent workers` option so that workers remain alive after each epoch’s dataset traversal, thereby avoiding repeated initialization and improving multi-epoch efficiency.

²Crucially, this counter is implemented as a *shared queue* to avoid race conditions arising from simultaneous updates by multiple threads. While Python’s GIL might suggest concurrency safety, a queue proves more robust in practice. The queue structure ensures: (1) exact correspondence between worker requests and server-propagated requests, and (2) a blocking mechanism that suspends workers until their response is ready from the local server. This design avoids potential update discrepancies that could occur with shared tensor implementations.

D Hyperparameters

D.1 Hyperparameter Search

We performed a grid search across two key hyperparameters for all methods: initial learning rates $\eta \in \{0.01, 0.02, 0.05, 0.1, 0.2, 0.3\}$ and adversarial factors $\rho \in \{0.1, 0.05, 0.01\}$. For LSAM, we explored the pulling strength formulation $\lambda = \frac{\lambda_0}{\eta\tau}$ with $\lambda_0 \in \{0.1, 0.2, 0.5, 0.9\}$, while fixing $\eta' = 1.0$ and momentum coefficient $\beta = 0.9$.

We note that in Algorithm 2, the learning rate η for the LSAM sampler adheres to standard SGD practices. Conversely, the optimization phase of LSAM uses a constant learning rate of 1.0 and mainly relies on the Nesterov-momentum-based gradient prediction, parameterized by β , to enable accelerated optimization.

D.2 Hyperparameter Selection

To achieve optimal performance across all experiments, we consistently applied two configurations:

- $\rho = 0.1$ for both LSAM and DP-SAM methods
- Architecture-specific learning rates: 0.02 for CNNs and 0.2 for ResNet, VGG, and WRN architectures across *all* methods

For LSGD (Teng et al., 2019) and EASGD (Zhang et al., 2015), in consistency with their original implementations, we maintain their default parameters.

E Additional Results

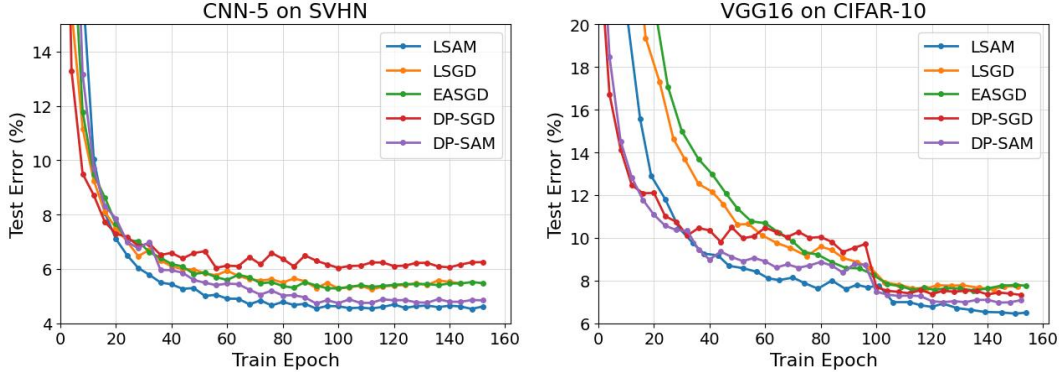


Figure 5: Test error versus train epoch on SVHN dataset.

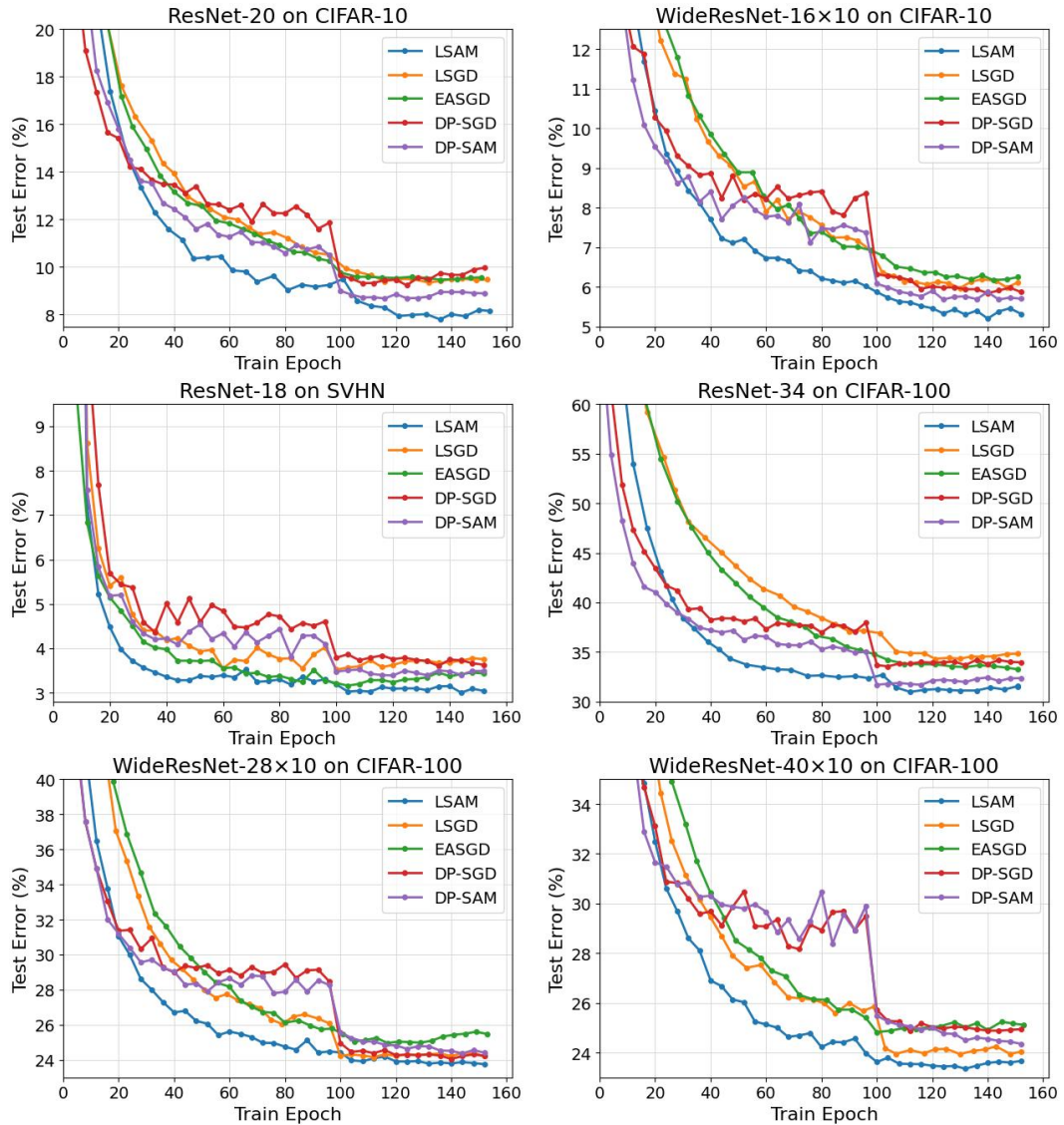


Figure 6: Test error versus train epoch on CIFAR-10 and CIFAR-100 datasets.